Peer-reviewed version available at *ISPRS Int. J. Geo-Inf.* **2020**, *9*, 512; doi:10.3390/ijgi9090512

Article

Catchment-Scale Flood Modelling in Data-Sparse Regions Using Open-Access Geospatial Technology

Iguniwari Thomas Ekeu-wei[1, 2*], and George Alan Blackburn[1]

[1]Lancaster Environment Centre, Lancaster University, Lancaster LA1 4YQ, United Kingdom; a.blackburn@lancaster.ac.uk
[2]Kawari Technical Services Nigeria Limited, Yenagoa, Nigeria.
*Correspondence: iguniwari@gmail.com; Tel.: +234-812-097-0000

Received: date; Accepted: date; Published: date

Abstract: Consistent data is seldom available for whole-catchment flood modelling in many developing regions, thus this study demonstrates how the complementary strengths of open and readily available geospatial datasets and tools can be leverage to map flood risk within acceptable levels of uncertainty for flood risk management. Available fragmented remotely-sensed and in situ datasets (including hydrological data, altimetry, digital elevation model, bathymetry, aerial photos, optical and radar imageries) are systematically integrated using 2-dimensional CAESAR-LISFLOOD model to quantify and recreate the extent and impact of the historic 2012 flood in Nigeria. Experimental modelling, calibration and validation is undertaken for the whole Niger-South hydrological catchment area of Nigeria, then segmented into sub-domains for re-validation to understand how data variability and uncertainties impact on the accuracy of model outcomes. Furthermore, aerial photos are applied for the first time in the study area for flood model validation and to understand how different physio-environmental properties influence synthetic aperture radar flood delineation capacity in the Niger Delta region of Nigeria.

Keywords: Open-access; geospatial; remote sensing; hydrodynamic model; CAESAR-LISFLOOD; data-sparse; and flood risk management.

1. Introduction

The magnitude and frequency of flood events are continuously increasing, owing to climate change and anthropogenic factors that exacerbate flood impact into the foreseeable future [1]. The total global cost of coastal and river flood damage in 2010 stood at US$ 46 trillion and is projected to increase to US$ 158 trillion by 2050 in business as usual conditions [2]. Factors such as population rise and urban sprawl towards floodplains also contribute to the high cost of flood disasters [3], especially in developing regions where urban planning regulations are less stringent, and the vulnerable are disproportionately affected by floods due to limited institutional and technical coping capacity, including limited data availability due to financial, institutional, operational and technical shortcomings [4].

Accurate information on flood magnitudes, including inundation extent, depth and propagation velocity are essential to inform flood risk management interventions [5]. Such information can are typically generated by flood modelling and mapping processes such as flood frequency analysis, hydrodynamic modelling and flood hazard mapping [6]. Flood frequency analysis estimates the return period of a flood of a specific magnitude, by fitting a defined probability distribution to historical annual maximum or partial discharge time series [7]. For ungauged or sparsely gauged rivers, alternative methods based on runoff estimation [8], empirical altimetry forecast rating curve extrapolation [9] and regionalization techniques [10] can be applied. Hydrodynamic modelling utilises topographic and bathymetric data that characterise river channel and floodplain terrain, as well as hydrographic data and Manning's roughness that defines terrain resistances, to derive flood water depth, extent and propagation velocity extent [11]. Lastly, flood hazard and vulnerability maps communicate physical and socio-economic exposure [12]. Flood maps can be presented in probabilistic

or deterministic formats, depending on the purpose, type of flood information and accompanying uncertainty to be communicated [13,14].

Typically, a network of river gauging stations is usually installed to acquire daily river hydrology data which is stored over time to provide historical timeseries [15]. However, logistics and financial challenges in developing countries limit the spatial coverage and density of gauge networks [16,17]. In some situations, even where gauging stations exist, data collected is often insufficient due to disruption of measuring infrastructure by intense flood events, poor planning, institutional and technological limitations [18,19]. Likewise, high-resolution ground survey and topography data (e.g. Light Detection and Ranging (LiDAR)) are cost intensive.

In many developing regions, flood modelling and mapping processes are hampered by lack of sufficient in situ data [20]. Such regions are termed "data-sparse", as it challenges flood modelling efforts and could flaw flood management interventions, and consequently aggravate flood impacts [20,21]. Advances in earth observation technology and availability of open-access remotely-sensed data over the past decades has drastically reduced the cost associated with hydrographic, topographic and landscape data collection, resulting in improved flood modelling and mapping [4,22]. Therefore, hydrologist and researchers alike have shifted focus to applying open-access remotely-sensed in data-sparse regions to bridge the data-gap and minimise the cost associated with data collection, flood modelling, calibration and validation [20,23,24]. Nonetheless, in many cases, these alternative open-access datasets are usually of insufficient spatial coverage for catchment-scale modelling owing to a range of physical, atmospheric and technological factors [22,25] and require systematic data integration is essential to draw maximum benefits from all available data.

This study explores an integrated approach for flood modelling and mapping, combining available segmented hydrographic, topographic, floodplain roughness, calibration and validation datasets using two-dimensional CAESAR-LISFLOOD-FP hydrodynamic model to quantify and recreate the extent and impact of the historic 2012 flood in Nigeria. The specific objectives of this study include:

1. To systematically harness open-access remotely-sensed and readily available geospatial data to improve catchment-scale flood modelling.
2. To explore the use of freely available aerial photos for flood model validation in vegetation dominant regions in comparison to Synthetic Aperture Radar (SAR);
3. To quantify the magnitude and impact of the devastating 2012 flood in Nigeria.

1.1. Study area

The study area, the Niger-South Hydrological Area 5 (Figure 1A) is located downstream of the 2,170,500 km^2 Niger river basin (Figure 1B), collecting an average annual discharge of 6000 m^3/s from 11 riparian countries [26] through the Niger and Benue rivers to the Atlantic Ocean via the Nun and Forcados distributaries in the Niger Delta region of southern Nigeria [27]. Due to these high flows, many rivers within the Niger basin are dammed for hydroelectric power generation, irrigation or flood control purposes [28,29]. In recent years the Niger and Benue Rivers have been heavily influenced by excess water released from upstream dams in Nigeria, Niger and Cameroon [30,31], resulting in flooding of the low-lying settlements within floodplains [32-34]. The annual average rainfall in the region varies from 750 to 1600mm, and the annual average temperature ranges from 18 to 28°C.

The flood model domain for this study is represented by the DEM presented in Figure 1, while the sub-domains with variable data availability are defined by the red rectangles to represent Lokoja, Onitsha and the Niger Delta. These sub-domains are selected for subsequent analysis and model re-validation to reflect varying data availability and geomorphological characteristics (i.e. river confluence, canyon and delta). The study area was amongst the most affected areas during the unprecedented 2012 flooding [30,31]. The convergence of excess water from Niger and Benue rivers initiated flooding at Lokoja confluence [34]; the Onitsha/Asaba floodplain was flooded due to high upstream flow from Lokoja and river channel constriction that resulted in backwater effect [35]; and the Niger Delta region was flooded as a result of its low-lying topography and the influx of rising upstream water levels Lokoja and Onitsha [31].

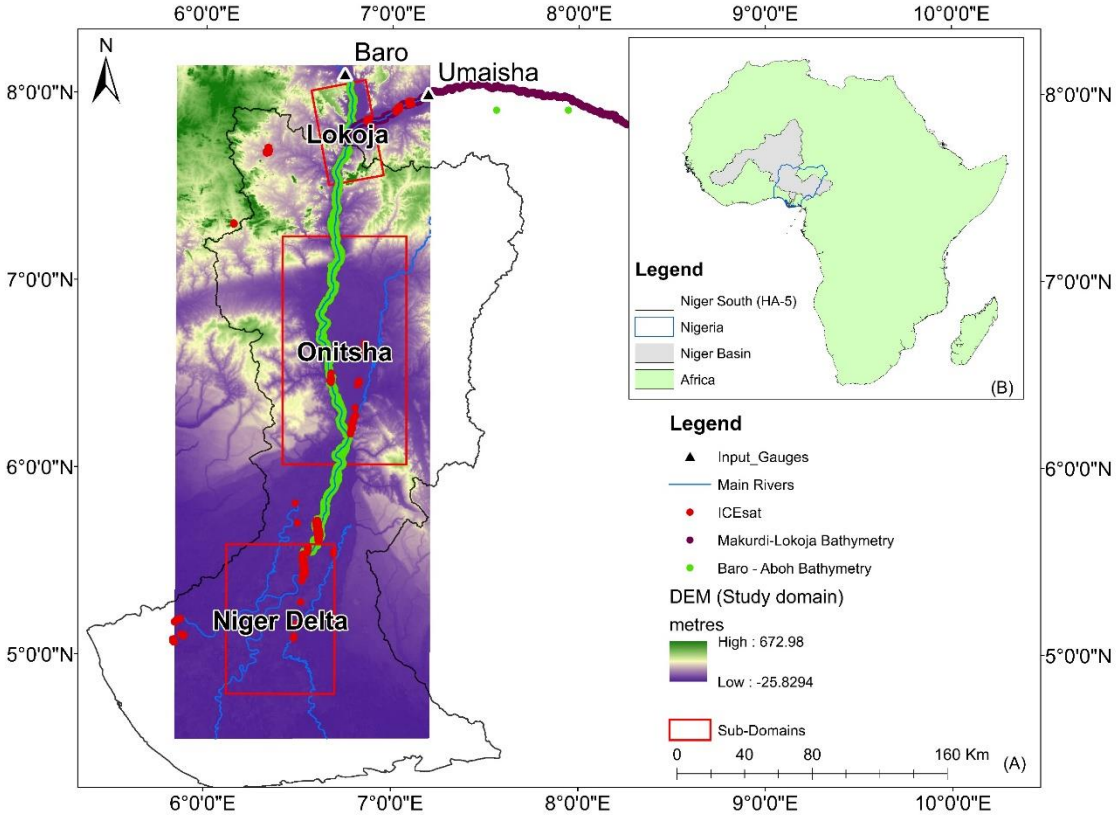

Figure 1 (A) Map of the study area, showing the Niger-South river basin (hydrological area 5), gauging stations, ICESat elevation points, bathymetry points, DEM/Model domain and sub-domains. Figure 1 (B) Map of Africa showing the Niger Basin that discharges through the HA-5 into the Atlantic Ocean.

2. Materials and Methods

2.1. Methodological Framework

A flowchart of the overall study methodology is presented in Figure 2, detailing how the various datasets including hydrographic, topographic, Manning's roughness characteristics and remotely sensed optical, radar, altimetry and aerial data are integrated for flood modelling and mapping. This study focuses on developing a model to quantify the magnitude, as well as recreate the extent and impact of the 2012 flood event; combining available data in every aspect of the flood modelling process in a way that reduces the uncertainty in the outcome.

Preprints (www.preprints.org) | NOT PEER-REVIEWED | Posted: 10 July 2020 doi:10.20944/preprints202007.0207.v1

Peer-reviewed version available at ISPRS Int. J. Geo-Inf. 2020, 9, 512; doi:10.3390/ijgi9090512

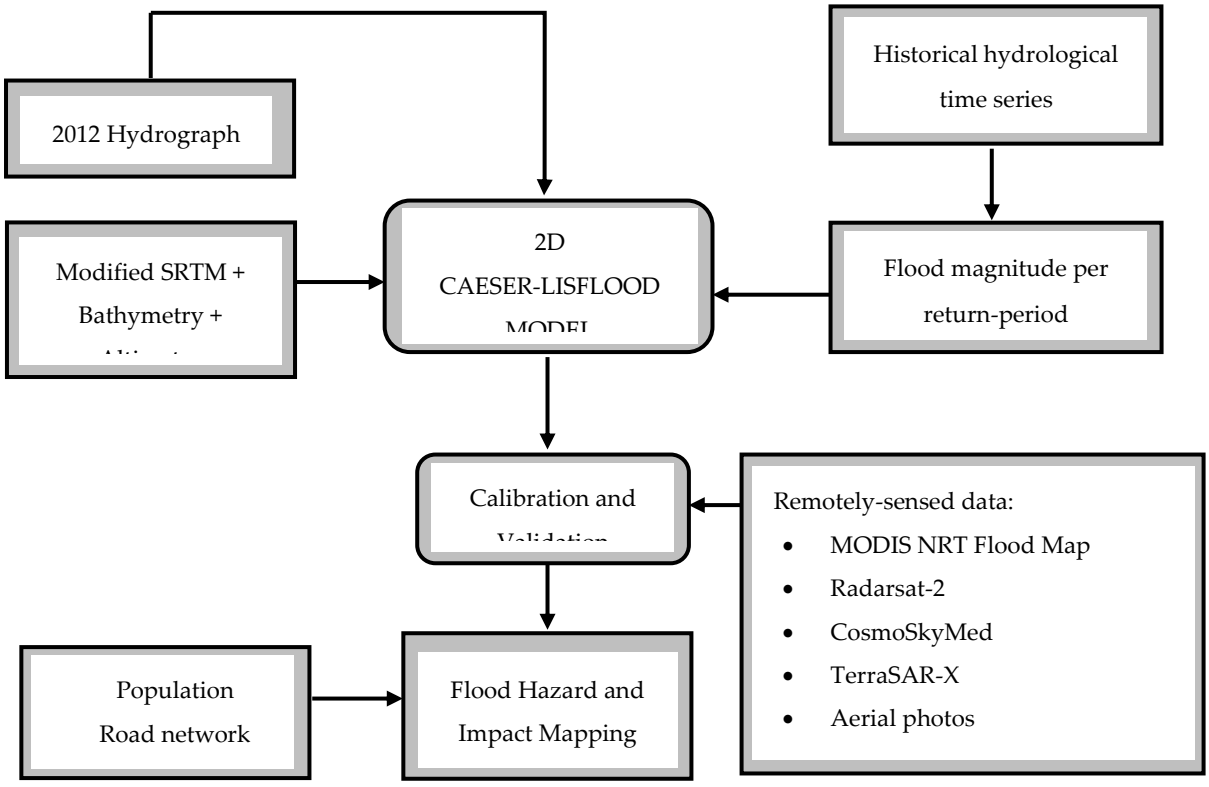

Figure 2 Conceptual flowchart of integrated flood modelling and mapping in the Niger South basin.

2.2. Datasets

Remotely-sensed imagery data are used in this study to assess how well the hydrodynamic model represent observed flood extent. TerraSAR-X, Moderate Resolution Imaging Spectroradiometer (MODIS) Near-Real-Time (NRT) flood maps, Radarsat-2 and CosmoSkyMed images corresponding with different time-points in the 2012 hydrograph (rise, peak and fall) are combined to compensate for the deficiencies of optical and radar images for flood extent delineation [22]. Properties of the imagery used, including dates of acquisition, upstream discharge and return periods are presented in Table 1. Table 2 shows the matrix of data availability across the three subdomains.

Table 1. Satellite imagery used in the study with acquisition dates and corresponding upstream gauge station discharge values and flood return periods.

Dates	Images and availability				Baro	Return Period	Umaisha	Return Period
[YYYY-MM-DD]	TSX	MDS	R2	CSKD	(m^3/s)	(1-in-year)	(m^3/s)	(1-in-year)
2012-09-03	×	√	√	×	5,187	2	12,303	2
2012-09-25	√	√	×	×	8,533	50	20,328	100
2012-10-09	×	√	√	×	6,969	5	17,378	50
2012-10-11	×	√	√	×	6,696	5	16,771	20
2012-10-12	×	√	√	×	6,504	5	16,520	20
2012-11-06	×	√	√	√	3,270	2	7,955	2

Legend: TSX = TerraSAR-X, MDS = MODIS, R2 = Radarsat-2, CSKD = CosmoSkyMed, Legend: √ = available, x = unavailable.

2.2.1. River Discharge and Flood Frequency Estimates: The 2012 flood hydrograph discharge values at Baro and Umaisha gauging stations along the Niger and Benue rivers respectively, are used as initial boundary conditions for the hydrodynamic model. These datasets were obtained from the

Nigerian Hydrological Service Agency (NIHSA) and flood frequency estimates is calculated using a methodology developed in a previous study for data-spare regions [36], and applies the Generalised Extreme Value probability distribution. Flood frequency plots for Baro and Umaisha gauging stations are presented in Figures S1 and S2 respectively (supplementary material).

2.2.2. Modified SRTM DEM: In the absence of high-resolution topography data, Shuttle Radar Topography Mission (SRTM) – Digital Elevation Model (DEM) have been widely applied for hydrodynamic modelling to provide a continuous terrain surface upon which flood is routed [21,37]. The SRTM C and X band SAR sensors were flown aboard the space shuttle Endeavour from February 11 to 22, 2000 through a joint mission between National Aeronautics and Space Administration (NASA) and National Geospatial-Intelligence Agency (NGA) to acquire near-global (80%) land elevation data of approximately 90 meters spatial resolution [38]. Despite the wide applicability of the SRTM DEM, its C and X-band radar cannot penetrate water surface and vegetation canopies to define underlying channel geometry and backscatter from urban roof-tops contributes to positively biased elevation estimates [23,37]. Modified SRTM DEMs by O'Loughlin et al. [39] and Sampson et al. [40] that correct for voids, vegetation and urban area reflection anomalies are used in this study. These DEMs are combined using the ArcGIS minimum mosaic function that returns the minimum cell value of two overlapping data cells as an output. This method assumes that the lowest DEM value represents bare earth elevation, thus curbing overestimation bias. A comparative analysis showing the improved accuracy of the modified SRTM DEMs is presented in Ekeu-wei and Blackburn [4].

2.2.3. River Bathymetry: Access to bathymetric data is restricted and, in some situations, sold at an exorbitant cost by custodians, thus creating artificial data scarcity. Bathymetric data are obtained from two sources, i) Digital Horizon Company Limited (2011): 240km river survey from Makurdi to Lokoja, collected using HYDROSTAR ELAC 4300 DUAL Echo-sounder and C-Nav 2050 differential GPS systems (see "Makurdi-Lokoja Bathymetry", Figure 1); ii) Royal Haskoning (2002): 300km river survey from Baro to Aboh (see "Baro-Aboh Bathymetry", Figure 1), collected using an Ashtech Z12 Real-Time Kinematics GPS, Navisound 210, Navisound 50 and Raytheon 210Kc digital and analogue echo sounders; and iii) In the absence if bathymetric data for the Niger Delta Sub-domain, the average vertical bias (difference) between ICESat-derived inland water surface spot heights and SRTM DEM is applied to modify the river channel geometry of the modified SRTM DEM [41]. All bathymetric data, ICESat and the modified SRTM are re-projected to the Mean Seal Level (MSL) vertical datum/UTM 32N and merged using the nearest neighbour method [42] to derive in a 90-metre resolution hydrologically smoothed DEM. The modified DEM is resampled from 90 to 270 metres, thereby reducing the number of cells to1,793,400 (active = 1,256,656) within a 9,1610 km^2 domain area, resulting in reduced computational cost and SRTM DEM noise [37], to meet CAESAR-LISFLOOD cell computation limit of fewer than 2 million cells.

2.2.4. Moderate Resolution Imaging Spectroradiometer (MODIS) Water Product (MWP): The Global 250 metres resolution Near-Real-Time (NRT) binary flood maps derived from combined MODIS bands 1, 2 and 7 using Dartmouth Flood Observatory algorithm [43] is applied to validate modelled flood extent. The MODIS instrument is onboard NASA's Terra and Aqua satellites provide twice-daily optical images which are automatically processed and made available as the MWP for download via http://oas.gsfc.nasa.gov/floodmap/ [44]. Only composite time-series of MWP imagery from September to October of 2012 that corresponded with time points of the 2012 hydrograph for peak river flow periods in Nigeria is used. The dates of the images used are presented in Table 1.

2.2.5. Synthetic Aperture Radar (SAR): SAR is widely applied in flood modelling and mapping studies as it provides all-weather day and night time high spatial and temporal resolution SAR images with varying polarization [22,25]. The SAR datasets used in this study include i) *Radarsat-2*: This C-Band satellite mission emerged from a collaboration between the Canadian Space Agency and MacDonald Dettwiler Associates Limited; ii) *CosmoSkyMed*: The Constellation of Small Satellites for

Mediterranean basin Observation (CosmoSkyMed) is a 4-spacecraft constellation conceived by Agenzia Spaziale Italiana, and funded by the Italian Ministry of Research and the Italian Ministry of Defense. Each of the four satellites is equipped with an X band SAR instrument; and iii) *TerraSAR-X*: This German Earth-observation satellite with X-band SAR sensor was launched on June 15 2007, and became fully operational by January 2008. It offers a wide range of beam modes, allowing it to record day and night-time images with different swath widths, resolutions, polarizations, and at varying incidence angles.

Radarsat-2 and CosmoSkyMed images were obtained from Shell Petroleum Development Company (SPDC), while flood extent from TerraSAR-X was acquired from the International Charter on Space and Major Disasters repository produced by the Regional Centre for Training in Aerospace Survey using images provided for Call 415 in 2012. The dates of the images used are presented in Table 1.

2.2.6. Aerial Photos: Optical satellite images are often hampered by cloud cover and only provide daytime images, while C and X band SAR and optical images alike are unable to penetrate vegetation canopies to delineate underlying flooding, hence underestimating flood extent [22,45]. Therefore, 287 geotagged aerial photos acquired by SPDC from a helicopter using a Nikon D7000 camera is used in this study. The photos were obtained for the Niger Delta sub-domain during the peak of flooding in 2012. These aerial photos are not ortho-corrected and lack the necessary meta for such pre-processing, hence are visual interpreted and manually classified as flooded (1) and non-flooded (0), then applied to extract corresponding flood conditions for the modelled and observed (SAR) flood extents for comparative analysis. The aerial photos were acquired from the helicopter at an average distance of approximately 2km from the focal point (Figure S3, supplementary material), therefore a 2 km buffer distance is created around the aerial photo data points and spatial zonal statistics applied to select the dominant (majority) cell value (flooded/non-flooded) contained within the buffer area from the outputs of the hydrodynamic model and SAR imagery flood extract. Aerial photo data points are applied to ground-truth modelled and observed (satellite) flood extent by a comparative analysis of the percentage of hits and misses.

2.2.7. Data for Flood Impact Evaluation: To assess the impact of the 2012 flood event, overlay analysis is performed to identify population and infrastructure (road network and built-up areas) exposure to observed and modelled (2012 and 1-in-100year) flood extent. The Gridded Population of the World (GPW)-v4 and Global Roads Open Access Data Set (gROADS) are acquired from the Socio-Economic Data and Application Centre database. Landsat-8 Operational Land Imager imagery (Path:189/Row:55) is used to map built-up Landuse, using a maximum likelihood supervised classification approach similar to Butt et al. [46].

Table 2: Spatial data availability matrix for sub-domains

Spatial Data	Data Source	Sub-Domains		
		Lokoja	Onitsha	Niger Delta
MODIS Water Product	Nigro [43]; NASA	√	√	×
TerraSAR-X	Disaster Charter	√	×	×
Radarsat-2	Ekeu-wei [36]; SPDC	×	×	√
Cosmo-SkyMed	Ekeu-wei [36]; SPDC	×	×	√
Aerial Photos	Ekeu-wei [36]; SPDC	×	×	√
Bathymetry	Royal Haskoning; Digital Horizon	√	√	×
ICESat	O'Loughlin et al., [41]	√	√	√
SRTM DEM	NASA and NGA	√	√	√
Legend: √ = available; x = unavailable,				

2.2. CAESAR-LISFLOOD (CL) Hydrodynamic Model Description and Setup

The CAESAR-LISFLOOD hydrodynamic and geomorphological modelling tool [47] embedded with the LISFLOOD-FP code [48] is selected for this study due to its applicability for fluvial flood

modelling in data-sparse regions, using coarse resolution terrain datasets [21,37,49]. The 2-Dimensional CAESAR-LISFLOOD grid discretized floodplain model calculates flow between two Cartesians coordinates (X and Y) driven by gravity because of the free surface height difference between two elevation cells. This is given by the equation:

$$\mathbf{Q} = \frac{\mathbf{q} - \mathbf{g}\mathbf{h}_{\mathbf{flow}}\Delta\mathbf{t}\frac{\Delta(\mathbf{h}+\mathbf{z})}{\Delta\mathbf{x}}}{(\mathbf{1} + \mathbf{g}\mathbf{h}_{\mathbf{flow}}\Delta\mathbf{t}\mathbf{n}^{\mathbf{2}}|\mathbf{q}|/\mathbf{h}_{\mathbf{flow}}^{\mathbf{10/3}})}\Delta\mathbf{x} \qquad (\mathbf{1})$$

where $\mathbf{Q}$ is defined as the flow between neighbouring cells, $\mathbf{q}$ is the flux (i.e. flow rate per unit area) between cells from previous time steps, $\mathbf{g}$ is the acceleration due to gravity, $\mathbf{n}$ is the Manning's roughness coefficient, $\mathbf{h}$ is the water depth, $\mathbf{z}$ is the bed elevation, $\mathbf{h}_{\mathbf{flow}}$ is the maximum flow depth difference between cells, $\Delta\mathbf{x}$ is the grid resolution, and $\mathbf{t}$ is time. The depth of water within each cell is defined by:

$$\frac{\Delta\mathbf{h}^{\mathbf{i,j}}}{\Delta\mathbf{t}} = \frac{\mathbf{Q}_{\mathbf{x}}^{\mathbf{i-1,j}} - \mathbf{Q}_{\mathbf{x}}^{\mathbf{i,j}} + \mathbf{Q}_{\mathbf{x}}^{\mathbf{i,j-1}} - \mathbf{Q}_{\mathbf{x}}^{\mathbf{i,j}}}{\Delta\mathbf{x}^{\mathbf{2}}} \qquad (\mathbf{2})$$

where $\mathbf{i}$ and $\mathbf{j}$ are the cell coordinates. The model time step controlled by the shallow water Courant-Friedrichs-Lewy (CFL) conditions is defined by:

$$\Delta\mathbf{t}_{\mathbf{max}} = \boldsymbol{\alpha}\frac{\Delta\mathbf{x}}{\sqrt{\mathbf{gh}}} \qquad (\mathbf{3})$$

Where $\boldsymbol{\alpha}$ is a coefficient (Courant number) that varies from 0.3 to 0.7 depending on the cell size and influences the model stability [50]. High values of $\boldsymbol{\alpha}$ increase the model time-step and reduce model runtime but can result in more unstable models. For this study, $\boldsymbol{\alpha}$ is approximated as 0.7 based on suggestions by Coulthard et al. [51] for cell size greater than 50 metres.

2.3. Model Calibration and Validation

Flood model calibration is usually undertaken by adjusting the predetermined manning's roughness (n) coefficient that depicts river channel and floodplain resistance to flow, while comparing flood model outcomes such as inundation extent and/or water depth to similarly known parameters obtained from other data sources such as radar altimetry, optical and radar satellite imagery [21,49], aerial photography [52] and/or *in situ* river measurements [11]. Calibration aims to assess the model's capacity to predict observed flood levels within acceptable levels of uncertainty [53]. Manning's roughness coefficient is typically predetermined based on existing literature [54,55], and assigned to represent the degree of flow resistance caused by varying land use/cover types. Depending on the level of details required, spatially distributed or static roughness values can be assigned to the model [56]. In this catchment-scale study, static manning's roughness is applied and varied from 0.01 to 0.045 to broadly capture the roughness of the Niger South hydrological area as defined by Olayinka [57], i.e. from clean smooth recently excavated/dredged sandy river to meandering river with obstructions, dunes large enough to cause cross-sectional turbulence.

F-Statistics, BIAS, and percentage (%) flood capture are the evaluation matrices used to compare the model to observed flood extent [24,53], and these parameters are defined as thus:

$$\mathbf{F} = \frac{\mathbf{A}}{\mathbf{A} + \mathbf{B} + \mathbf{C}} \qquad (\mathbf{4})$$

Where A = (Simulated wet and observed wet), B = (Simulated wet but observed dry), C = (Simulated dry but observed wet) and D = (Simulated dry and observed dry) are defined in Table 3, and F can range from 0 to 1, increasing in levels of accuracy.

Model BIAS and percentage of observed flood correctly captured are stipulated as:

$$\mathbf{BIAS} = \frac{\mathbf{A} + \mathbf{B}}{\mathbf{A} + \mathbf{C}} \quad (\mathbf{5})$$

$$\%\ \mathbf{Flood\ Capture} = \frac{\mathbf{A}}{\mathbf{A} + \mathbf{C}} \quad (\mathbf{6})$$

Multiple simulations of the CAESER-LISFLOOD model is run for the whole model domain due to the availability of gauging stations upstream (See Baro and Umaisha in Figure 1) as an upstream boundary condition while varying static Manning's roughness coefficients from 0.01 to 0.045 at intervals of 0.005. The modelled flood extent is compared to the observed satellite flood extent to assess model performance using the aforementioned matrices. The model is also re-validated for the sub-domains, to capture the data and landscape variability impact on the flood model outcome.

3. Results and Discussion

3.1. Integration of open-access remote sensing and geospatial data for catchment-scale flood modelling

Figure 3 shows the model performances in relation to varied manning's roughness coefficient "n" from 0.01$m^{1/3}S^{-1}$ to 0.045$m^{1/3}S^{-1}$, suggesting 0.04$m^{1/3}S^{-1}$ as the optimal manning's roughness coefficient, given that model's F-statistic begin to decline at "n" value of 0.045 $m^{1/3}S^{-1}$. The optimal Manning's roughness used is consistent with a previous study in the same study area [58], where optimal channel and over-bank manning's roughness coefficient of 0.04 was adopted for the one-dimensional SOBEK model. Some description of roughness parameters within the channel and floodplain include matured crops, scattered bush, heavy weeds, short grass, early growth vegetation, sand dune and meandering channel [54,55]. Also, it can be observed that the model performance improves when re-evaluated as sub-domains rather than when treated as a whole domain. This performance variation is consistent with data quality variation, decreasing downstream of the study domain. Similar model performance variation was observed by Skinner et al. [11], where model performance uncertainty increased with data ambiguity.

In Table 3 and 4, the model performance is evaluated against Optical and combined Optical+Radar imageries at Lokoja, Onitsha and the Niger Delta sub-domains. The model appears to perform better when evaluated against the combined Optical+Radar flood extent, in contrast to only MODIS optical imagery. The combination of optical and radar imagery has been widely reported to improve flood extent delineation and is particularly useful for large-scale flood monitoring [59]. At Lokoja sub-domain, a minimal difference is observed between the model F-statistic when evaluated against optical MODIS imagery and TerraSAR-X flood extents, i.e. 0.729 and 0.808 respectively, owing to the limited cloud and vegetation cover in the region. In the Niger Delta sub-domain dominated by seasonal cloud cover due to nearness to the Atlantic coast, the combination of RADARSAT2+ CosmoSkyMed images resulted in improved model predictiveness of 0.187, from 0.095 for optical MODIS only, as well as an overall reduction in BIAS. This improvement can be attributed to SAR sensors ability to penetrate cloud cover to delineate underlying flood. Notwithstanding, the relatively low F-statistic values despite the improvement suggest the presence of high model uncertainty in the region, attributed to input variables limitations, such as SRTM DEM, as well as SAR image deficiency in the mangrove-dominated regions [45]. The overall F-statistics for the whole model domain is found to be generally low (Figure 4, Tables 5 and 6), owing to data uncertainty that propagates from input to processes, to flood model outcome [60]. This data effectiveness/uncertainty effect is further revealed in the sub-domains, where the model predictiveness assessment pervades the effect of spatial data disparity as previously disclosed. The flood extent BIAS and the percentages of flood captured in Tables 4 and 5 also corresponded to the variability of data across the overall domain and sub-domains.

Peer-reviewed version available at ISPRS Int. J. Geo-Inf. 2020, 9, 512; doi:10.3390/ijgi9090512

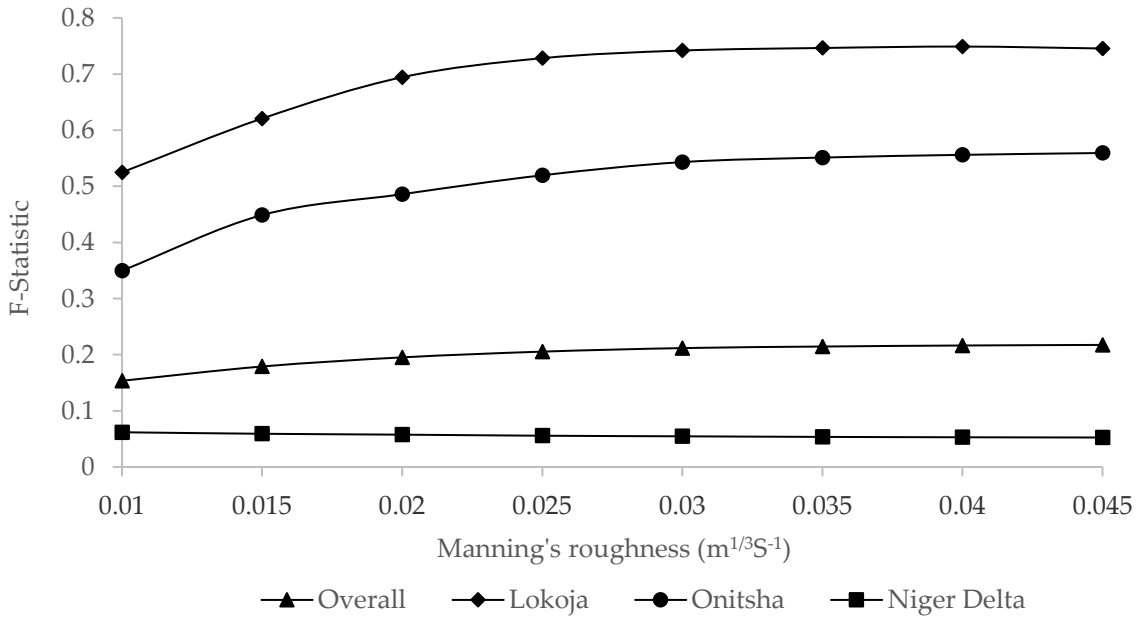

Figure 3 Plot of Model Performance Criteria (F-Statistic) versus Manning's roughness (n)

Table 3. Performance Matrices for optimal manning's roughness (0.04 $m^{1/3}S^{-1}$) calibration (MODIS).

Performance	Overall	Lokoja	Onitsha	Niger Delta
F	0.235	0.729	0.534	0.095
BIAS	4.245	1.183	1.140	9.661
% Flood Capture	99.972	92.012	74.545	92.186

Table 4. Performance Matrices for optimal manning's roughness (0.04 $m^{1/3}S^{-1}$) calibration (TerraSAR-X/MODIS/RADARSAT2/CosmoSkyMed).

Performance	Overall	Lokoja	Onitsha	Niger Delta
F	0.273	0.808	0.529	0.187
BIAS	2.511	0.918	1.132	3.432
% Flood Capture	75.308	85.679	73.802	69.946

On establishing that the best fit CAESER-LISFLOOD model outcome is characterised by a static manning's roughness coefficient of 0.04$m^{1/3}S^{-1}$, it can be observed that the modelled flood extent patterns for the three sub-domains are consistent with those observed from satellite imagery (Figure 4 (A-C)) and reflects the data variability effect as defined by the performance matrices, with model outcome uncertainty (over-estimation) increasing downstream as data availability reduces.

Detailed floodplain and river terrain characterization have been identified as inputs that influence the outcomes of hydrodynamic models [61,62]. SRTM DEM combined with up-to-date (2011) river bathymetric data at Lokoja resulted in a model performance of F=0.8, a matrix consistent with other studies where DEM and Bathymetry data integration emanated in improved model outcomes [21,56,63]. At Onitsha, where SRTM is combined with obsolete bathymetric data acquired in 2002, before dredging activities in 2010 [64], F=0.5 is achieved, hence the bathymetric data likely over-estimated the river depth, consequently resulting in an over-estimated modelled flood extent (Figure 4B). A reduced model accuracy of approximately F=0.2 in the Niger Delta sub-domain is attributed to the lack of bathymetry data in the flat terrain area, resulting in simplified river geometry characterization which does not explicitly capture river network details such as anabranches and meandering, thus causing flood model over-estimation due to the ease of water conveyance from shallow rivers to adjacent floodplains [65,66]. Also, unregulated sand mining activities, water-

saturated mangrove and poor dredging and debris management practices are likely factors that contribute to the model uncertainty within the region [27], as they could influence and trigger hydrological and hydraulic changes.

Furthermore, previous studies in the region based on global flood models such as CaMa-UT, GLOFRIS, JRC, ECMWF, SSBN, and CIMA-UNEP [40,67,68], presented similar inundation pattern, but slightly less model to observation agreement at Lokoja, Onitsha and the Niger Delta decreasing downstream from the deep and narrow rivers with constricted floodplains to the shallow rivers and low-lying floodplains of the Niger Delta wetland that is difficult to characterize using coarse terrain data such as the SRTM DEM [67]. Given that some local data such river bathymetry and other validation datasets were available this study, which is seldom available for global flood models [67,69,70], the outcomes of this study is considerably better than global models.

Overall, the flood pattern displayed in Figure 4(A-C) is consistent with the geomorphology of the sub-domains and its influence on the hydraulics of the catchment areas. For instance, at Lokoja sub-domain, flood spreads out at the confluence in Lokoja where the Niger and Benue rivers meet and propagate towards floodplains; at Onitsha, extended flood areas can be observed, attributed to back-water effect caused the constricted river channel at Asaba that deflects water to fill the dish-like relatively flat floodplain [68]; and the widespread flooding across the Niger Delta region can be linked to the low-lying topography of the region, as well as the inability of the shallow rivers (Nun and Forcados) to contain the excess water coming from upstream rivers (Niger and Benue). These characteristics suggest that enhanced river channel and floodplain topography characterization is essential for shallow channels and low-lying floodplains [71].

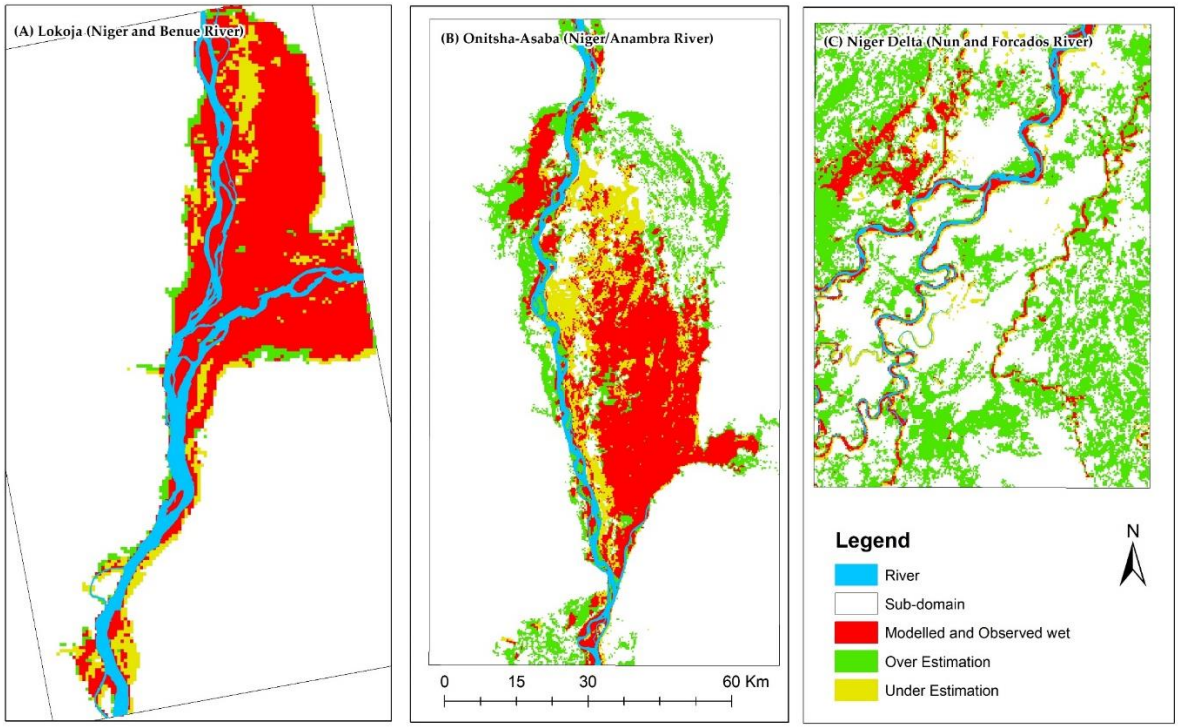

Figure 4 Lokoja (A), Onitsha-Asaba (B) and Niger Delta (C) CAESAR-LISFLOOD Model outcome and satellite (Combined MODIS and SAR) observation comparison.

3.2. Flood model re-validation in vegetation dominant region using freely available aerial photos and SAR

The combination of optical and radar satellite resulted in the improved model to observation agreement as seen in Table 3 and 4, Figure 4 (A-C). However, SAR is known to be deficient in mangrove, swamps and built-up areas [22,45], as depicted by the observed minimal change in model performance from 0.095 to 0.187 when comparing the model to optical and radar+optical images derived flood extents respectively in the Niger region dominated by mangrove vegetation.

Peer-reviewed version available at ISPRS Int. J. Geo-Inf. 2020, 9, 512; doi:10.3390/ijgi9090512

To better assess the model's performance in the Niger Delta sub-domain where SAR is known to be deficient, aerial photo data points acquired during the 2012 flood event is applied for the first time, and the results are presented in Figure 5 (A-D) and Table 5. Figure 6 shows images some of the aerial photo data points distributed across the typical environmental/physical landscape variations in the Niger Delta region, i.e. (A) mixed land use (built-up area greater than vegetation); (B) mixed land use (vegetation greater than built-up); (C) bare land, sparsely built and vegetated lands; and (D) matured mangrove vegetation. These physio-environmental variations are known to influence SAR inundation delineation capacities and hydrodynamic model performance [72], as seen in Table 5, where higher level of agreement is observed between aerial photo data points and model (69%), compared to SAR (13%). This outcome further buttressing SAR's deficiency in delineating flooding in mangrove dominated regions, as well as the potential limitation of SRTM DEM to under or over-estimate terrain elevation for hydrodynamic modelling [73,74]. In conclusion, this assessment provides a novel approach to ascertain the deficiencies of hydrodynamic models and SAR images in complex terrains using aerial photos. Nevertheless, better value can be extracted from such data if the spatial distribution is improved, and the data is collected to enable ortho-correction for pixel or area-based comparative analysis.

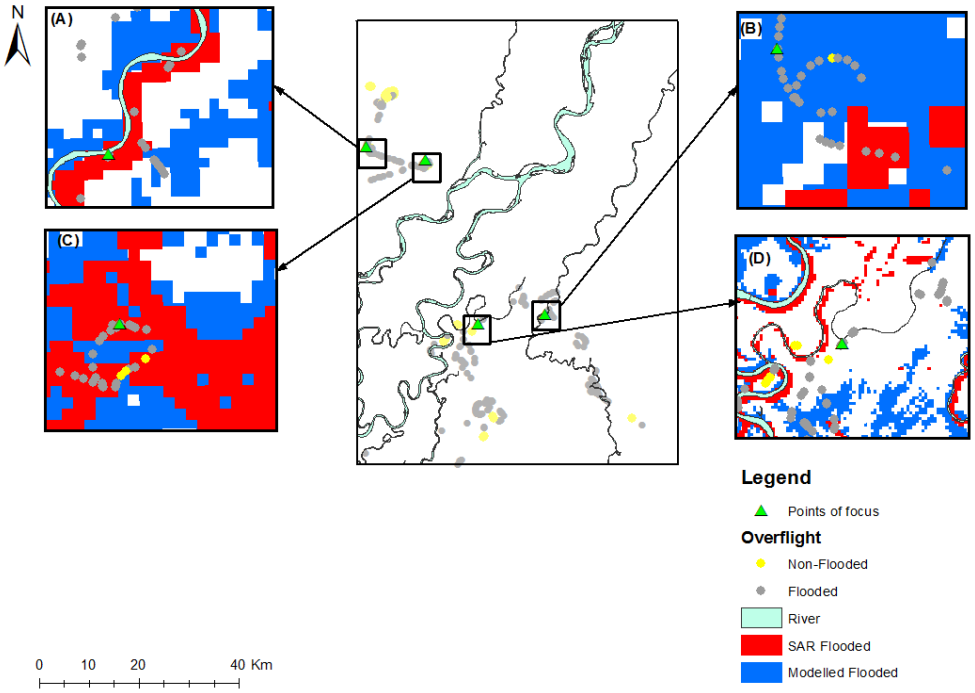

Figure 5 Niger Delta aerial geotagged photo points comparison with model and SAR observation outcomes (Photos for green points of focus shown in Figure 8).

Peer-reviewed version available at ISPRS Int. J. Geo-Inf. 2020, 9, 512; doi:10.3390/ijgi9090512

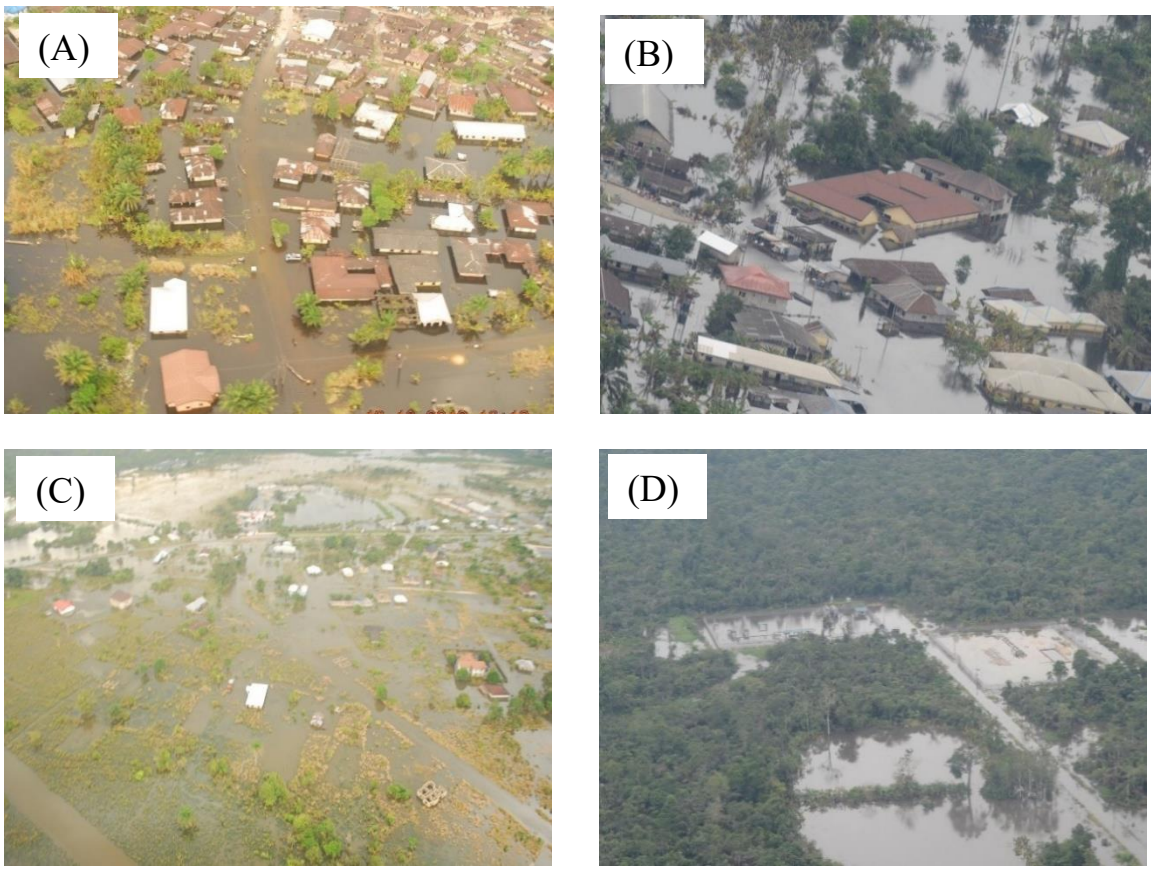

Figure 6 Sectional examples of aerial photos of flooded areas compared to observed and modelled flood in the Delta region, showing points of focus (Figure 7). (A) = match between model and photo, (B) = match between SAR and photo, (C) = match between model, SAR and photo, (D) = only the aerial photo showing flooding.

Table 5. Comparative analysis of aerial photo data points, model and SAR observation flood extents.

Points of focus	Data Points (n = 287)	Hits	Miss	% Accuracy
A	Aerial photo and Model flooded	196	91	69
B	Aerial photo and SAR flooded	37	250	13
C	Aerial photo, Model and SAR flooded	43	244	15
D	The aerial photo only flooded	62	-	-

3.3. Quantifying the magnitude and impact of the 2012 flood in Nigeria

The 1-in-100year flood recommended by the Technical Guidelines on Soil Erosion, Flood and Coastal Zone Management [75] for flood risk management in Nigeria is estimated at 13,887 and 19,589 m^3/s for Baro and Umaisha gauging stations along Niger and Benue rivers respectively, based on a methodology developed from a previous study [36]. These estimates are applied to retrospectively quantify the impact of the 2012 flood event at Lokoja sub-domain, where the highest model performance is observed, for inundated land area, population, built-up areas and roads. Similar impact assessment is also undertaken using peak flood magnitude of 2012 (Figure S4, supplementary material) and the results are presented alongside observed satellite flood extent in Table 6 and Figure 7 (A-B).

The areas observed as flooded by satellite imagery is consistent with modelled flooded areas for a 1-in-100year flood and the peak flood of 2012 (Figure 7), resulting in more than 95% spatial extent agreement. Furthermore, similarities are visible for observed and modelled flood impact for the exposed land area, population, built-up area, and major roads displayed in Table 6. These indicators are relevant to understand the exposure to flooding, impact to infrastructure, evacuation strategy, as well as damage to households and livelihoods to inform future flood risk management interventions.

Preprints (www.preprints.org) | NOT PEER-REVIEWED | Posted: 10 July 2020 doi:10.20944/preprints202007.0207.v1

Peer-reviewed version available at ISPRS Int. J. Geo-Inf. 2020, 9, 512; doi:10.3390/ijgi9090512

Table 6 Model Observed and 1-in-100-year flood exposure comparisons

Flood	Area (km²)	Population	Built-up (km²)	Roads (km)
2012 Model	425.8	32,703	12.648	34.573
1-in-100 year modelled	427.2	32,867	12.834	32.987
2012 Observed (Satellite)	440.2	34,391	12.326	37.287

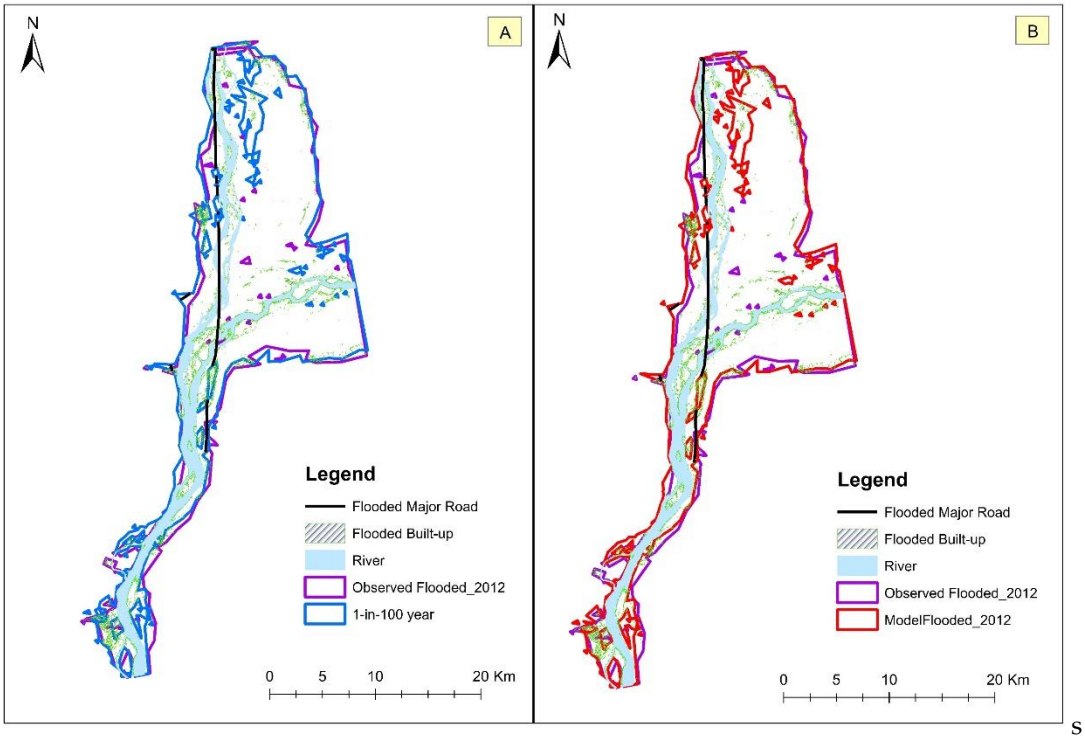

Figure 7 (A) comparison of SAR observed 2012 and 1-in-100-year modelled flood extents, and (B) comparison of SAR observed 2012 and modelled flood extents for the same period, as well as impacted land area, roads and built-up areas in both A and B at Lokoja.

4. Conclusions

In this study, an integrated approach of harnessing open-access remote sensing and geospatial data is presented, to improve flood modelling and mapping processes in data-sparse regions. Our approach systematically combines freely available historical hydrological data, SRTM DEM, bathymetric survey, aerial photos, optical and Synthetic Aperture Radar (SAR) imageries, drawing from the advantages of open-access and readily available datasets, as well as highlighting their deficiencies and opportunities for data enhancement to improve flood modelling and mapping.

The spatial extent of open-access remotely-sensed data is rarely sufficient or uniformly available for catchment-scale modelling in many developing regions; thus, the result of this study indicates that the combination of up-to-date hydrological, river bathymetry, SRTM DEM, optical and radar satellite images provide the optimal data for considerably improved flood modelling and mapping. Also, researchers in developing countries need to be more innovative in data sourcing especially as several relevant datasets are restricted or sold at an exorbitant price by custodians. Efforts should be out to partner with public and private institutions to enable access to commercially acquired or restricted datasets that are useful to flood modelling and mapping processes, as well as leverage on open-data initiatives such as Open Data Program by DigitalGlobe (now Maxar) and consortiums like the International Disaster Charter.

The deficiency of remotely sensed data for flood modelling and mapping is further revealed in SAR sensor's inability to efficiently delineate flooding in the vegetated Niger Delta region, as well as the reduced depiction of river geometry by SRTM DEM, resulting in the over-estimation of flooding in the Onitsha and Niger Delta sub-domains. The uncertainties associated with these datasets impact

on flood model to observation agreement. Also, the importance of using up-to-date bathymetric data for flood modelling is demonstrated, especially for shallow floodplains as seen in the various sub-domains, where the use of 2011, 2002 and non-existent bathymetry data at Lokoja, Onitsha and the Niger Delta respectively resulted in consistently decreasing model accuracy. The application of aerial geotagged photos presents an innovative approach for flood model validation in vegetation dominated and coastal regions where optical and radar satellite imagery flood detection capacity is impaired by vegetation and cloud cover. Street-level georeferenced imagery is widely collected for post-flood impact assessment in data-spare regions and could prove vital for flood model calibration and validation [76].

The retrospective recreation of the 2012 flood event at Lokoja sub-domain helped quantify the event as a 1-in-100year flood, matching the spatial extent of the peak and modelled flood extent by a goodness of fit of over 95%, and is comparable to global flood models from a recent study in the same sub-domain [68]. The approach demonstrated in this study if harnessed with the current virtual network of radar altimetry stations along Niger and Benue [77], as well as improvements in in-situ observatory through programmes such as Nigeria Erosion and Watershed Management Project (NEWMAP) and Transforming Irrigation Management in Nigeria (TRIMING) would improve climate information services in Nigeria. Furthermore, proactive identification of locations at risk of flooding and safe dry areas for emergency response coordination during an extreme event becomes feasible, thereby complementing the national annual flood outlook report of NIHSA that suggest locations likely to be flooded with no spatially quantifiable parameter (e.g. flood extent) to inform intervention decisions.

Supplementary Materials: The following are available online at www.mdpi.com/xxx/s1, Figure S1: Baro flood frequency plot; Figure S2: Umaisha flood frequency plot; Figure S3: Model, Observation and Overflight line of sight overlaid on high-resolution GeoEye Imagery; and Figure S4: Input hydrographs at the upstream boundaries of Umaisha and Baro.

Author Contributions: I.T.E and G.A.B conceptualized the study; I.T.E. performed the collected the data, designed the methodology and undertook the analysis (hydrodynamic analysis, flood modelling and mapping) and validation under the supervision G.A.B; I.T.E. drafted this Manuscript, and G.A.B reviewed, edited and provided constructive feedback and inputs for improvement.

Funding: The authors acknowledges funding from the Niger Delta Development Commission (NDDC), Nigeria for Iguniwari Thomas Ekeu-wei's PhD study at Lancaster University, United Kingdom (NDDC/ DEHSS/ 2013 PGFS/BY/5).

Acknowledgments: We acknowledge (i) Engr. Clement Nze of the Nigerian Hydrological Service Agency for providing the in-situ river hydrological data and advice for hydrological analysis; (ii) Shell Petroleum Development Company for providing the Radarsat-2, CosmoSkyMed, and aerial geotagged datasets, and Mr Chituru Obowu for his technical guidance; (iii) the Dartmouth Flood Observatory for the NRT MODIS Flood maps; (iv) Digital Horizon Company Nigeria Limited and Royal Haskoning for providing the Bathymetry datasets. We also extend thanks to Dr Mark Trigg of the School of Civil Engineering, University of Leeds, UK, and Prof. Tamunoene Kingdom Simeon Abam of the Institute of Geoscience and Space Technology, River State University of Science and Technology, Nigeria, for their valuable advice during this study.

Conflicts of Interest: The authors declare that they have no competing interests.

References

1. Balbus, J.M.; Boxall, A.B.A.; Fenske, R.A.; McKone, T.E.; Zeise, L. Implications of global climate change for the assessment and management of human health risks of chemicals in the natural environment. Environmental Toxicology and Chemistry 2013, 32, 62-78, doi:10.1002/etc.2046.
2. Jongman, B.; Ward, P.J.; Aerts, J.C.J.H. Global exposure to river and coastal flooding: Long term trends and changes. Global Environmental Change 2012, 22, 823-835, doi:10.1016/j.gloenvcha.2012.07.004.
3. Yukiko, H.; Roobavannan, M.; Sujan, K.; Lisako, K.; Dai, Y.; Satoshi, W.; Hyungjun, K.; Shinjiro, K. Global flood risk under climate change. Nature Climate Change 2013, 3, 816, doi:10.1038/nclimate1911.

4. Ekeu-wei, I.T.; Blackburn, G.A. Applications of Open-Access Remotely Sensed Data for Flood Modelling and Mapping in Developing Regions. Hydrology, 2018; Vol. 5, p 39.
5. Els, Z. Data availability and requirements for flood hazard mapping. PositionIT. Master of Natural Sciences at Stellenbosch University 2013.
6. Aerts, J.C.J.H.; Alphen, J.v.; Moel, H.d. Flood maps in Europe-methods, availability and use. Natural Hazards and Earth System Sciences 2009, 9, 289-301.
7. Reed, D. Procedures for flood freequency estimation, Volume 3: Statistical procedures for flood freequency estimation; Institute of Hydrology: 1999.
8. Rogger, M.; Kohl, B.; Pirkl, H.; Viglione, A.; Komma, J.; Kirnbauer, R.; Merz, R.; Blöschl, G. Runoff models and flood frequency statistics for design flood estimation in Austria – Do they tell a consistent story? Journal of Hydrology 2012, 456-457, 30-43, doi:10.1016/j.jhydrol.2012.05.068.
9. Pandey, R.; Amarnath, G. The potential of satellite radar altimetry in flood forecasting: concept and implementation for the Niger-Benue river basin. Proc. IAHS 2015, 370, 223-227.
10. Haddad, K.; Rahman, A.; Ling, F. Regional flood frequency analysis method for Tasmania, Australia: A case study on the comparison of fixed region and region-of-influence approaches. Hydrological Sciences Journal 2014, doi:10.1080/02626667.2014.950583.
11. Skinner, C.J.; Coulthard, T.J.; Parsons, D.R.; Ramirez, J.A.; Mullen, L.; Manson, S. Simulating tidal and storm surge hydraulics with a simple 2D inertia based model, in the Humber Estuary, U.K. Estuarine, Coastal and Shelf Science 2015, 155, 126-136, doi:10.1016/j.ecss.2015.01.019.
12. Kron, W. Flood risk= hazard• values• vulnerability. Water International 2005, 30, 58-68.
13. Di Baldassarre, G.; Schumann, G.; Bates, P.; Freer, J.; Beven, K. Flood- plain mapping: a critical discussion of deterministic and probabilistic approaches. Hydrological Sciences Journal 2010, 55, 364-376, doi:10.1080/02626661003683389.
14. Domeneghetti, A.; Vorogushyn, S.; Castellarin, A.; Merz, B.; Brath, A. Probabilistic flood hazard mapping: effects of uncertain boundary conditions. Hydrology and Earth System Sciences 2013, 17, 3127-3140, doi:10.5194/hess-17-3127-2013.
15. Bshir, D.; Garba, M. Hydrological monitoring and information system for sustainable basin management. In Proceedings of First Annual conference of the Nigerian Association of Hydrological Sciences (2 - 4 December, 2003), Federal University of Technology, Yola, Adamawa, Nigeria.
16. Ngene, B.U. Optimization of rain gauge stations in Nigeria. Federal University of Technology, Owerri., Nigeria, 2009.
17. Ekeu-wei, I.T. Evaluation of Hydrological Data Collection Challenges and Flood Estimation Uncertainties in Nigeria. Environment and Natural Resources Research 2018, 8, 44 - 54, doi:10.5539/enrr.v8n2p44.
18. Olayinka, D.N.; Nwilo, P.C.; Emmanuel, A. From Catchment to Reach: Predictive Modelling of Floods in Nigeria. 2013.
19. Ngene, B.U.; Agunwamba, J.C.; Nwachukwu, B.A.; Okoro, B.C. The Challenges to Nigerian Raingauge Network Improvement. RJEES 2015, 7, 68-74, doi:10.19026/rjees.7.2205.
20. Yan, K.; Di Baldassarre, G.; Solomatine, D.P.; Schumann, G.J.P. A review of low-cost space-borne data for flood modelling: topography, flood extent and water level. Hydrological Processes 2015.
21. Sanyal, J.; Carbonneau, P.; Densmore, A. Hydraulic routing of extreme floods in a large ungauged river and the estimation of associated uncertainties: a case study of the Damodar River, India. Nat Hazards 2013, 66, 1153-1177, doi:10.1007/s11069-012-0540-7.

22. Musa, Z.; Popescu, I.; Mynett, A. A review of applications of satellite SAR, optical, altimetry and DEM data for surface water modelling, mapping and parameter estimation. Hydrology and Earth System Sciences Discussions 2015, 12, 4857-4878.
23. Yan, K.; Tarpanelli, A.; Balint, G.; Moramarco, T.; Baldassarre, G.D. Exploring the Potential of SRTM Topography and Radar Altimetry to Support Flood Propagation Modeling: Danube Case Study. J. Hydrol. Eng. 2015, 20, 04014048, doi:10.1061/(ASCE)HE.1943-5584.0001018.
24. Stephens, E.; Schumann, G.; Bates, P. Problems with binary pattern measures for flood model evaluation. Hydrological Processes 2014, 28, 4928-4937, doi:10.1002/hyp.9979.
25. Mason, D.C.; Schumann, G.; Bates, P. Data utilization in flood inundation modelling; Blackwell Publishing Ltd, Oxford, England: 2011; pp. 209-233.
26. Gaston, L. Integrated future needs and climate change on the River Niger water availability. Journal of Water Resource and Protection 2013, 2013.
27. Abam, T. Regional hydrological research perspectives in the Niger Delta. Hydrological Sciences Journal-Journal Des Sciences Hydrologiques 2001, 46, 13-25, doi:10.1080/02626660109492797.
28. Aich, V.; Koné, B.; Hattermann, F.F.; Müller, E.N. Floods in the Niger basin – analysis and attribution. Natural Hazards and Earth System Sciences Discussions 2014, 2, 5171-5212, doi:10.5194/nhessd-2-5171-2014.
29. Andersen, I.; Golitzen, K.G. The Niger river basin: A vision for sustainable management; World Bank Publications: 2005.
30. Ojigi, M.; Abdulkadir, F.; Aderoju, M. Geospatial mapping and analysis of the 2012 flood disaster in central parts of Nigeria. In Proceedings of 8th National GIS Symposium. Dammam; pp. 1-14.
31. Olojo, O.O.; Asma, T.I.; Isah, A.A.; Oyewumi, A.S.; Adepero, O. The Role of Earth Observation Satellite during the International Collaboration on the 2012 Nigeria Flood Disaster. In Proceedings of 64th International Astronautical Congress 2013, Abuja, Nigeria.
32. The Federal Government of Nigeria. Post-Disaster Needs Assessment 2012 Floods; 2013.
33. Agada, S.; Nirupama, N. A serious flooding event in Nigeria in 2012 with specific focus on Benue State: a brief review. Nat Hazards 2015, 77, 1405-1414, doi:10.1007/s11069-015-1639-4.
34. Odunuga, S.; Adegun, O.; Raji, S.; Udofia, S. Changes in flood risk in Lower Niger-Benue catchments. Proceedings of the International Association of Hydrological Sciences 2015, 370, 97.
35. Efobi, K.; Anierobi, C. Urban Flooding and Vulnerability of Nigerian Cities: A Case Study of Awka and Onitsha in Anambra State, Nigeria. Journal of Law, Policy and Globalization 2013, 19, 58-64.
36. Ekeu-wei, I.T. Application of open-access and 3rd party geospatial technology for integrated flood risk management in data sparse regions of developing countries. Lancaster University, Lancaster, UK, 2018.
37. Neal, J.; Schumann, G.; Bates, P. A subgrid channel model for simulating river hydraulics and floodplain inundation over large and data sparse areas. Water Resources Research 2012, 48.
38. Farr, T.G.; Rosen, P.A.; Caro, E.; Crippen, R.; Duren, R.; Hensley, S.; Kobrick, M.; Paller, M.; Rodriguez, E.; Roth, L., et al. The Shuttle Radar Topography Mission. Reviews of Geophysics 2007, 45, n/a-n/a, doi:10.1029/2005RG000183.
39. O'Loughlin, F.; Paiva, R.; Durand, M.; Alsdorf, D.; Bates, P. Development of a'bare-earth'SRTM DEM product. In Proceedings of EGU General Assembly Conference Abstracts; p. 9651.
40. Sampson, C.C.; Smith, A.M.; Bates, P.D.; Neal, J.C.; Alfieri, L.; Freer, J.E. A high- resolution global flood hazard model. Water Resources Research 2015, 51, 7358-7381, doi:10.1002/2015WR016954.

41. O'Loughlin, F.E.; Neal, J.; Yamazaki, D.; Bates, P.D. ICESat-derived inland water surface spot heights. Water Resources Research 2016, 52, 3276–3284, doi:10.1002/2015WR018237.
42. Sibson, R. A brief description of natural neighbour interpolation. Interpreting multivariate data 1981, 21, 21-36.
43. Nigro, J.; Slayback, D.; Policelli, F.; Brakenridge, G. NASA/DFO MODIS Near Real-Time (NRT) Global Flood Mapping Product Evaluation of Flood and Permanent Water Detection. 2014.
44. Revilla-Romero, B.; Hirpa, F.A.; Thielen-Del Pozo, J.; Salamon, P.; Brakenridge, R.; Pappenberger, F.; De Groeve, T. On the Use of Global Flood Forecasts and Satellite- Derived Inundation Maps for Flood Monitoring in Data- Sparse Regions. Remote Sensing 2015, 7, 15702-15728, doi:10.3390/rs71115702.
45. Long, S.; Fatoyinbo, T.E.; Policelli, F. Flood extent mapping for namibia using change detection and thresholding with sar. Flood extent mapping for Namibia using change detection and thresholding with SAR 2014, 9, 035002, doi:10.1088/1748-9326/9/3/035002.
46. Butt, A.; Shabbir, R.; Ahmad, S.S.; Aziz, N. Land use change mapping and analysis using Remote Sensing and GIS: A case study of Simly watershed, Islamabad, Pakistan. The Egyptian Journal of Remote Sensing and Space Science 2015, 18, 215 - 259.
47. Van De Wiel, M.J.; Coulthard, T.J.; Macklin, M.G.; Lewin, J. Embedding reach-scale fluvial dynamics within the CAESAR cellular automaton landscape evolution model. Geomorphology 2007, 90, 283-301, doi:10.1016/j.geomorph.2006.10.024.
48. Bates, P.D.; Horritt, M.S.; Fewtrell, T.J. A simple inertial formulation of the shallow water equations for efficient two-dimensional flood inundation modelling. Journal of Hydrology 2010, 387, 33-45, doi:10.1016/j.jhydrol.2010.03.027.
49. Trigg, M.A.; Bates, P.D.; Wilson, M.D.; Horritt, M.S.; Alsdorf, D.E.; Forsberg, B.R.; Vega, M.C. Amazon flood wave hydraulics. Journal of Hydrology 2009, 374, 92-105, doi:10.1016/j.jhydrol.2009.06.004.
50. Almeida, G.A.M.; Bates, P.; Freer, J.E.; Souvignet, M. Improving the stability of a simple formulation of the shallow water equations for 2- D flood modeling. Water Resources Research 2012, 48, n/a-n/a, doi:10.1029/2011WR011570.
51. Coulthard, T.J.; Neal, J.C.; Bates, P.D.; Ramirez, J.; de Almeida, G.A.M.; Hancock, G.R. Integrating the LISFLOOD-FP 2D hydrodynamic model with the CAESAR model: implications for modelling landscape evolution. Earth Surface Processes and Landforms 2013, 38, 1897-1906, doi:10.1002/esp.3478.
52. Neal, J.; Schumann, G.; Fewtrell, T.; Budimir, M.; Bates, P.; Mason, D. Evaluating a new LISFLOOD-FP formulation with data from the summer 2007 floods in Tewkesbury, UK. Journal of Flood Risk Management 2011, 4, 88-95.
53. Di Baldassarre, G. Floods in a changing climate [electronic resource] : inundation modelling; Cambridge : Cambridge University Press: 2012.
54. Chow, V. Open Channel Hydraulics; McGraw-Hill: New York 1959.
55. Arcement, G.J.; Schneider, V.R. Guide for selecting Manning's roughness coefficients for natural channels and flood plains. US Government Printing Office Washington, DC, USA: 1989.
56. Seenath, A. Modelling coastal flood vulnerability: Does spatially-distributed friction improve the prediction of flood extent? Applied Geography 2015, 64, 97-107, doi:10.1016/j.apgeog.2015.09.010.
57. Olayinka, D.N. Modelling Flooding in The Niger Delta. Lancaster University, 2012.
58. Musa, Z.N.; Popescu, I.I.; Munett, A. Sensitivity Analysis of the 2D SOBEK Hydrodynamic Model of the Niger River. In Proceedings of The 36th IAHR World Congress, 28 June –3 July, 2015, The Hague, the Netherlands.

59. Tong, X.; Luo, X.; Liu, S.; Xie, H.; Chao, W.; Liu, S.; Liu, S.; Makhinov, A.; Makhinova, A.; Jiang, Y. An approach for flood monitoring by the combined use of Landsat 8 optical imagery and COSMO-SkyMed radar imagery. ISPRS Journal of Photogrammetry and Remote Sensing 2018, 136, 144-153.

60. Jung, Y.; Merwade, V. Estimation of uncertainty propagation in flood inundation mapping using a 1-D hydraulic model. Hydrological Processes 2015, 29, 624-640, doi:10.1002/hyp.10185.

61. Cook, A.; Merwade, V. Effect of topographic data, geometric configuration and modeling approach on flood inundation mapping. Journal of Hydrology 2009, 377, 131-142, doi:10.1016/j.jhydrol.2009.08.015.

62. Jarihani, A.A.; Callow, J.N.; McVicar, T.R.; Van Niel, T.G.; Larsen, J.R. Satellite- derived Digital Elevation Model (DEM) selection, preparation and correction for hydrodynamic modelling in large, low- gradient and data- sparse catchments. Journal of Hydrology 2015, 524, 489-506, doi:10.1016/j.jhydrol.2015.02.049.

63. Casas, A.; Benito, G.; Thorndycraft, V.R.; Rico, M. The topographic data source of digital terrain models as a key element in the accuracy of hydraulic flood modelling. Earth Surface Processes and Landforms 2006, 31, 444-456, doi:10.1002/esp.1278.

64. Van Der Burg, T. Dredging for development on the lower river Niger between Baro and Warri, Nigeria; 2010.

65. Md Ali, A.; Solomatine, D.P.; Md Ali, G.; Solomatine, G.; Di Baldassarre, G. Assessing the impact of different sources of topographic data on 1- D hydraulic modelling of floods. Hydrology and Earth System Sciences 2015, 19, 631-643, doi:10.5194/hess-19-631-2015.

66. Domeneghetti, A.; Tarpanelli, A.; Brocca, L.; Barbetta, S.; Moramarco, T.; Castellarin, A.; Brath, A. The use of remote sensing- derived water surface data for hydraulic model calibration. Remote Sensing of Environment 2014, 149, 130-141, doi:10.1016/j.rse.2014.04.007.

67. Trigg, M.; Birch, C.; Neal, J.; Bates, P.; Smith, A.; Sampson, C.; Yamazaki, D.; Hirabayashi, Y.; Pappenberger, F.; Dutra, E. The credibility challenge for global fluvial flood risk analysis. Environmental Research Letters 2016, 11, 094014.

68. Bernhofen, M.V.; Whyman, C.; Trigg, M.A.; Sleigh, A.; Smith, A.M.; Sampson, C.C.; Yamazaki, D.; Wars, P.J.; Rudari, R.; Pappenberger, F., et al. A first collective validation of global fluvial flood models for major floods in Nigeria and Mozambique. Environmental Research Letters 2018.

69. Dottori, F.; Salamon, P.; Bianchi, A.; Alfieri, L.; Hirpa, F.A.; Feyen, L. Development and evaluation of a framework for global flood hazard mapping. Advances in Water Resources 2016, 94, 87-102, doi:10.1016/j.advwatres.2016.05.002.

70. Fleischmann, A.; Paiva, R.; Collischonn, W. Can regional to continental river hydrodynamic models be locally relevant? A cross-scale comparison. Journal of Hydrology 2019, doi:https://doi.org/10.1016/j.hydroa.2019.100027.

71. Gessese, A.; Wa, K.M.; Sellier, M. Bathymetry reconstruction based on the zero-inertia shallow water approximation. Theoretical and Computational Fluid Dynamics 2013, 27, 721-732.

72. Sanyal, J.; Densmore, A.L.; Carbonneau, P. Analysing the effect of land-use/cover changes at sub-catchment levels on downstream flood peaks: A semi-distributed modelling approach with sparse data. Catena 2014, 118, 28-40.

73. O'Loughlin, F.E.; Paiva, R.C.D.; Durand, M.; Alsdorf, D.E.; Bates, P.D. A multi- sensor approach towards a global vegetation corrected SRTM DEM product. Remote Sensing of Environment 2016, 182, 49-59, doi:10.1016/j.rse.2016.04.018.

74. Baugh, C.A.; Bates, P.D.; Schumann, G.; Trigg, M.A. SRTM vegetation removal and hydrodynamic modeling accuracy. Water Resources Research 2013, 49, 5276-5289, doi:10.1002/wrcr.20412.

75. Federal Ministry of Environment. Technical Guidelines on Soil Erosion, Flood and Coastal Zone management; 2005.

76. Yu, D.; Yin, J.; Liu, M. Validating city- scale surface water flood modelling using crowd- sourced data. Validating city-scale surface water flood modelling using crowd-sourced data 2016, 11, 124011, doi:10.1088/1748-9326/11/12/124011.

77. Biancamaria, S.; Hossain, F.; Lettenmaier, D.P. Forecasting transboundary river water elevations from space. Geophysical Research Letters 2011, 38, n/a-n/a, doi:10.1029/2011GL047290.